nature physics

JUNE 2018 VOL 14 NO 6
www.nature.com/naturephysics

Learned degrees

COMPLEX NETWORKS
Optimal inference

ENTANGLEMENT
Purely holographic

ROTATIONAL SPECTROSCOPY
Sympathetic cooling for high precision

nature physics

LETTERS

https://doi.org/10.1038/s41567-018-0074-3

Rotational spectroscopy of cold and trapped molecular ions in the Lamb–Dicke regime

Nature Physics 14, 555 -559 (2018), 10.1038/ s41567-018-0074-3

S. Alighanbari[1], M. G. Hansen[1], V. I. Korobov[2] and S. Schiller[1*]

Sympathetic cooling of trapped ions has been established as a powerful technique for the manipulation of non-laser-coolable ions[1–4]. For molecular ions, it promises vastly enhanced spectroscopic resolution and accuracy. However, this potential remains untapped so far, with the best resolution achieved being not better than 5×10^{-8} fractionally, due to residual Doppler broadening being present in ion clusters even at the lowest achievable translational temperatures[5]. Here we introduce a general and accessible approach that enables Doppler-free rotational spectroscopy. It makes use of the strong radial spatial confinement of molecular ions when trapped and crystallized in a linear quadrupole trap, providing the Lamb–Dicke regime for rotational transitions. We achieve a linewidth of 1×10^{-9} fractionally and 1.3 kHz absolute, an improvement of ≃50-fold over the previous highest resolution in rotational spectroscopy. As an application, we demonstrate the most precise test of ab initio molecular theory and the most accurate (1.3×10^{-9}) determination of the proton mass using molecular spectroscopy. The results represent the long overdue extension of Doppler-free microwave spectroscopy of laser-cooled atomic ion clusters[6] to higher spectroscopy frequencies and to molecules. This approach enables a wide range of high-accuracy measurements on molecules, both on rotational and, as we project, vibrational transitions.

Rotational spectroscopy of gas-phase molecules is a time-honoured technique that has been fundamental for developing our knowledge of molecular structure[7]. Its range continues to be extended (in the laboratory, in astronomical observatories and in space instruments), for example, to cold molecules[8]. Nevertheless, rotational spectroscopy has, in the majority of cases, not been able to achieve ultrahigh spectroscopic resolution and accuracy. Enabling this would open up numerous opportunities for studies in molecular physics and in fundamental physics, such as tests of molecular quantum theory, measurement of magnetic and optical susceptibilities, investigation of collision interactions, tests of the time-independence of particle masses[9–13], and the measurement of fundamental constants[5,14–16].

In conventional (linear) rotational spectroscopy, resolution can be improved by cooling of the molecules to a cryogenic translational temperature T, but the gains possible with thermal cooling methods ($T\simeq10$ K) are modest[8], due to the $\sqrt{T}$-dependence of the Doppler linewidth. For untrapped, neutral molecules, a leap in resolution and accuracy in rotational spectroscopy was achieved with the introduction of Lamb-dip (saturation) spectroscopy[17,18]. It allowed the fractional line resolution to be improved by approximately a factor of 20–30 beyond the Doppler broadening, to 5×10^{-8} (ref. [17]). However, this level has not improved for nearly 50 years[19,20], because it is limited by time-of-flight broadening. In the context of molecular ions, ion trapping combined with sympathetic cooling by Doppler-laser-cooled atomic ions to the 'crystallized' cluster state provides a well-tested approach for further reducing T to the 10 mK level, with a concomitant reduction of the Doppler linewidth by approximately a factor 30 (ref. [5]).

Here, we not only realize this improvement for rotational spectroscopy but also achieve Doppler-free spectral resolution, by reaching the rotational Lamb–Dicke regime (LDR). The LDR is defined by $\delta x<\lambda/2\pi$, where δx is the range of the ions' motion along the spectroscopy beam direction $\hat{\mathbf{k}}||x$ (ref. [21]), and λ is the radiation wavelength. In prolate ion clusters of appropriate size, the ranges of motion orthogonal to the clusters' long axes (z) are δx, $\delta y<20$ μm. Directing $\hat{\mathbf{k}}$ orthogonal to z satisfies the LDR condition for rotational transition wavelengths, with typical values $\lambda_{\rm rot}\simeq0.2$–2 mm. Ultrahigh fractional and absolute frequency resolutions are thereby enabled. In contrast, vibrational spectroscopy, where wavelengths are $\lambda_{\rm vib}<8$ μm, yields lines exhibiting the classic Doppler width[5,22], often further complicated by unresolved hyperfine structure[15,16]. The presented method does not require complex techniques such as single-ion manipulation, ground-state cooling and quantum spectroscopy[23,24] to capitalize on the advantage of the LDR regime. The performance improvement in terms of fractional resolution is a factor of ≃50 compared to both previous trapped molecular ion ensemble spectroscopy[5,22] and to the highest-resolution rotational spectroscopy of neutral molecules reported so far[20], to the best of our knowledge.

To perform a stringent test of the new method, we choose the polar molecule with the smallest fundamental rotational transition wavelength $\lambda_{\rm rot,min}\simeq228$ μm ($f_{\rm rot,max}\simeq1.3$ THz): HD^+ in its ground electronic state ($^2\Sigma_g^+$). In addition, the feasibility of ab initio calculation of $f_{\rm rot}$ for HD^+ and of its sensitivities to external fields allows the spectroscopic accuracy of the method to be tested.

The basic concept is depicted in Fig. 1. In a prolate ion cluster of appropriate size, trapped in a linear quadrupole trap (trap axis is along z), the sympathetically cooled ions arrange approximately as a narrow tube aligned along the trap axis. Maximum ion radial distances from the axis are significantly smaller than the tube length. Molecular dynamics simulations for a cluster containing $N=200$ HD^+ ions (Cluster 1, see Methods) indicate r.m.s. transverse position variations (corresponding approximately to the range $\delta x/2$) $\Delta x=\Delta y\simeq8.4$ μm at $T=12$ mK, increasing slightly to 9.0 μm at 67 mK. These values are significantly smaller than $\lambda_{\rm rot}/2\pi\simeq36$ μm, indicating the LDR if $\hat{\mathbf{k}}$ is chosen perpendicular to the trap axis. For a more quantitative treatment, we estimate the spectroscopy line shape L induced by the ions' motion, neglecting recoil and spontaneous emission effects, by evaluating the ensemble-averaged Fourier spectrum of the spectroscopy wave's electric field amplitude seen by each moving ion, $E(\mathbf{r}_i,\,t)\propto{\rm Re}[\exp(i\Phi(\mathbf{r}_i(t))-i\omega t)]$, where

[1]Institut für Experimentalphysik, Heinrich-Heine-Universität Düsseldorf, Düsseldorf, Germany. [2]Bogoliubov Laboratory of Theoretical Physics, Joint Institute for Nuclear Research, Dubna, Russia. *e-mail: step.schiller@hhu.de

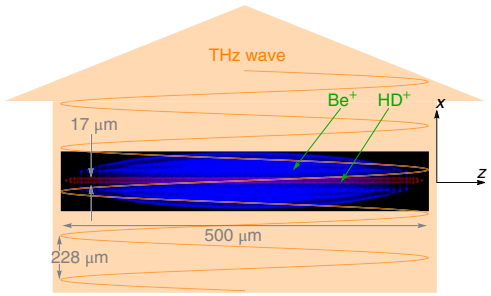

Fig. 1 | Principle of the Lamb–Dicke rotational spectroscopy of sympathetically cooled molecular ions. The ion cluster is prolate, and the sympathetically cooled ions exhibit a relatively small motional range in the directions *x*, *y* perpendicular to the trap axis *z*. The spectroscopy radiation propagates perpendicular to *z*. The ion cluster image is a time average of ion trajectories obtained from a molecular dynamics simulation of an ensemble of $N = 200$ HD^+ ions and $N_{Be^+} = 2,000$ atomic ions (see Methods). Ion clusters generated in the experiment are similar to the one shown here.

$\Phi(\mathbf{r}_i) = \mathbf{k} \cdot \mathbf{r}_i$. For transverse excitation along x, $\Phi(\mathbf{r}_i) = 2\pi x_i/\lambda$. We define $L(\Delta f) = \langle |\mathcal{F}_{\Delta f}\{\exp(i2\pi x_i(t)/\lambda)\}|^2 \rangle$, where the argument Δf of the Fourier transform $\mathcal{F}$ corresponds to the spectroscopic detuning from resonance and $x_i(t)$ are obtained from the molecular dynamics simulations and $\langle \ldots \rangle$ denotes the ensemble average. As shown in Fig. 2c, for $\lambda \leq 10\,\mu m$ (dashed lines) the line shape is close to Gaussian, with the full width at half maximum (FWHM) Δf_{FWHM} determined by the classic expression proportional to $\sqrt{T}$. For wavelengths $\lambda \geq 50\,\mu m$, the line shape shows features directly related to the x-coordinate spectral density (Fig. 2a), such as the drop for detunings larger than the secular frequency. In particular, because of the decreasing relative range with increasing λ and with decreasing temperature, a substantial delta function peak $L(0)$ (Lamb–Dicke peak) develops at $\Delta f = 0$. It is given by $L(0) = \langle |\exp(i2\pi x_i(t)/\lambda)| \rangle^2$ (the over-bar denotes the time average) and is shown in detail in Fig. 2d (points) as a function of wavelength. For the present wavelength $\lambda_{rot} \simeq 230\,\mu m$, nearly the complete line strength is in the Lamb–Dicke peak.

In the LDR, the absence of Doppler broadening and, because of ion confinement, also of transit-time broadening, puts into evidence other broadening mechanisms. However, pressure (collision) broadening can be suppressed by operating under ultrahigh-vacuum (UHV) conditions. Collisions between the trapped ions themselves do not lead to appreciable frequency shifts or broadening, because minimum approach distances are of the order of 10 μm. To reduce power (saturation) broadening below the 10^{-10} level for a typical strong transition, even for f_{rot} as high as 10^{12} Hz, extremely low power must be used (picowatt level).

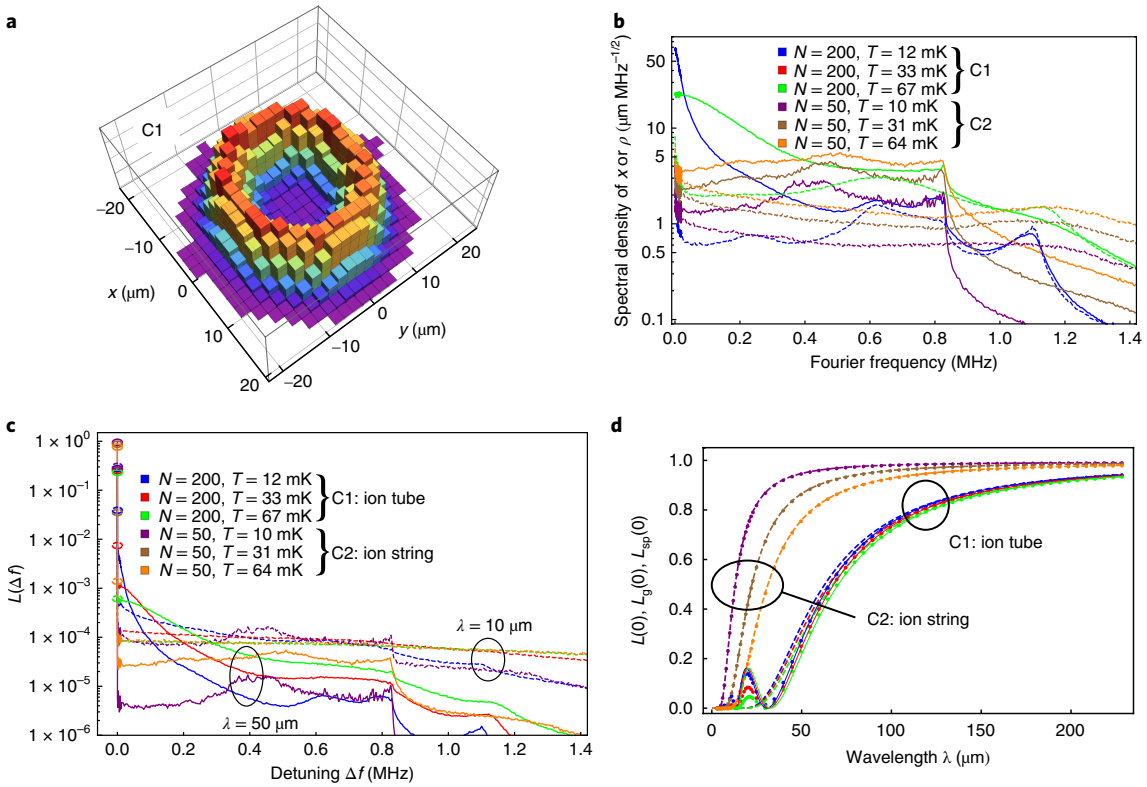

Fig. 2 | Characteristics and consequences of the motion of molecular ions in laser-cooled Be^+/HD^+ Coulomb clusters at different temperatures. Cluster C1 (C2): $N = 200(50)$, $N_{Be^+} = 2,000(500)$. The blue lines correspond to the situation in the experiment. **a**, Compound histogram of the transverse positions (x_i, y_i) of five randomly chosen molecular ions in cluster 1, at $T \simeq 33$ mK; the ring shape is related to the fact that, for the chosen ion numbers, the molecular ions arrange and move in a tubular cylindrical structure ('ion tube'). **b**, Ensemble average of the linear spectral density of the x coordinate of the ions (solid lines) and of the distance from the trap axis, $\rho = (x^2 + y^2)^{1/2}$ (dashed lines). The two spectra reflect the fact (evidenced by inspecting the ions' trajectories) that the transverse ion motion is a combination of a fast and small-range random motion perpendicular to the 'tube' axis, described by $\rho_i(t)$, and of a slower azimuthal motion around the tube, having a wider range. **c**, Qualitative spectral line shape $L(\Delta f)$, for two different wavelengths $\lambda = 50\,\mu m$ (solid lines), 10 μm (dashed lines). Only the positive detunings are shown. **d**, Strength of the Lamb–Dicke peak ($\Delta f = 0$). Points: exact values $L(0)$; dashed and solid lines: approximate expressions $L_g(0)$, $L_{sp}(0)$, respectively, defined in the Methods. The same colours in **b**–**d** correspond to the same cluster type and temperature. The transverse secular frequency of the molecular ions is 0.81 MHz; a corresponding feature is seen in the spectra of x and in the line shapes L.

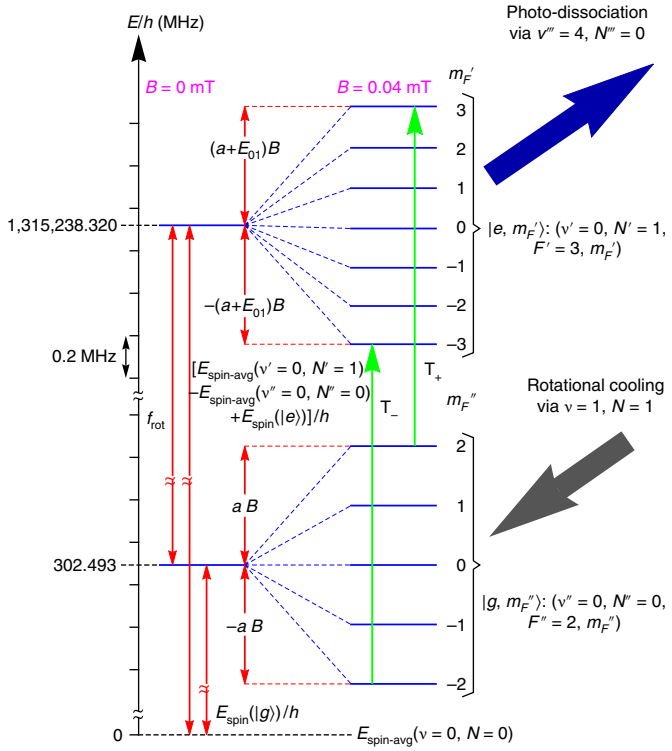

Fig. 3 | Simplified diagram of relevant energy levels of HD^+ in the ground vibrational level $v = 0$ of the $^2\Sigma_g^+$ electronic state. We show only one spin state, $F'' = 2$, of the ground rotational level $N'' = 0$, denoted by $|g\rangle$, and one spin state, $F' = 3$, of the first excited rotational level $N' = 1$, denoted by $|e\rangle$. The green arrows show the transitions $T_\pm$ addressed in this work, exhibiting a linear, and very small Zeeman splitting $2E_{01}B$. The population of the $N'' = 0$ spin states is enhanced by rotational cooling (thick grey arrow), and the population in the $N' = 1$ states is photo-dissociated by two lasers (blue arrow). The zero of the energy scale corresponds to the energy of the $v = 0$, $N = 0$ level in absence of the effective spin Hamiltonian interaction of ref. [33].

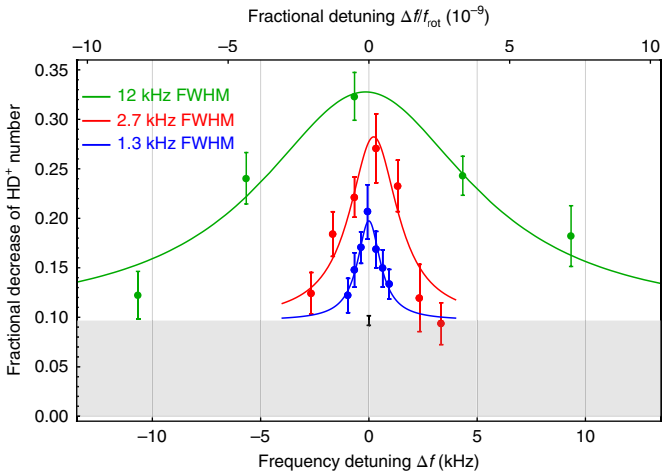

Fig. 4 | Spectroscopy of one hyperfine component of the fundamental rotational transition of HD^+. The unresolved transition pair $T_\pm$ between the stretched states, $(F'' = 2, m_{F''} = \pm F'') \rightarrow (F' = 3, m_{F'} = \pm F')$, at different power levels of the terahertz wave. The magnetic field is $B = 0.040(6)$ mT, measured with an anisotropic magnetoresistive probe and by radiofrequency spectroscopy of the Be^+ ions using the method of ref. [34]. The black error bar (the result of 500 experimental cycles) and the corresponding grey box indicate the background signal. The error bars are the standard error of the mean and the lines are Lorentzian fits. Zero detuning corresponds to the centre frequency of the blue fit.

Ultranarrow transitions may be challenging to find. Theoretical predictions and results from, for example, lower-resolution rovibrational spectroscopy may be helpful or necessary to reduce the spectral range of the search. Furthermore, performing the spectroscopy initially at high intensity leads to broad spectral lines, which are easier to find. The appropriate source power is easily satisfied by commercial devices.

To experimentally access the smallest possible linewidths, it is necessary to lift the Zeeman degeneracy of transitions by applying a magnetic field. Excitation of an individual Zeeman component implies excitation of only those molecules populating a single quantum state. Techniques for increasing the population in this state and thus the signal may therefore be required. Here, we use rotational laser cooling (see Methods).

The potential of rotational spectroscopy in the LDR can be harnessed fully only if the microwave source has excellent spectral purity (small linewidth) and high absolute frequency stability. For this work, we have implemented a frequency chain, where $f_{\mathrm{rot}} \simeq 1.3$ THz is referenced to a hydrogen maser (see Methods).

We address one particular spin component of the rotational transition, $|g\rangle = (v'' = 0, N'' = 0, F'' = 2) \xrightarrow{1.3\ \mathrm{THz}} |e\rangle = (v' = 0, N' = 1, F' = 3)$ of the ground electronic state $^2\Sigma_g^+$ (see Fig. 3). v, N and F denote the vibrational, rotational and total angular momentum quantum number, respectively. More precisely, we focus on two Zeeman components, T_+: $m_{F''} = 2 \rightarrow m_{F'} = 3$ and T_-: $m_{F''} = -2 \rightarrow m_{F'} = -3$ (m_F is the projection of the total angular momentum on the quantization axis). These connect so-called spin-stretched states (maximal F and m_F) and are advantageous for precision measurements because their Zeeman shift is strictly linear and tiny, $\Delta f_{\mathrm{rot,Zeeman}} = \pm E_{10}(v = 0,\ N = 1)B = \pm 5.6\,\mathrm{kHz}(B/1\,\mathrm{mT})$ (ref. [25] and Methods). The mean frequency of T_+ and T_- is therefore free of any Zeeman shift. We computed the frequency ab initio using the most advanced techniques available (see Methods); in zero magnetic field

$$f_{\mathrm{rot,theory}} = 1,314,935.8273(10)_{\mathrm{theo}}\ \mathrm{MHz} \quad (1)$$

Spectroscopy is performed by $1 + 1' + 1''$ resonance-enhanced multi-photon dissociation, where the upper spectroscopy level undergoes $|e\rangle \xrightarrow{1.42\ \mu\mathrm{m}} (v''' = 4,\ N''' = 0,\ F''' = 2) \xrightarrow{266\ \mathrm{nm}} \mathrm{H} + \mathrm{D}^+$. The reduction in the number of trapped HD^+ following dissociation is measured using secular excitation, and represents the spectroscopy signal. Repeated HD^+ trap loading and spectroscopy cycles are performed and the signals are averaged so as to increase the signal-to-noise ratio. Typical ion clusters used for spectroscopy are similar to the one shown in Fig. 1, having $T \simeq 10$ mK.

Figure 4 shows the measured spectrum $|g\rangle \rightarrow |e\rangle$ in the neighbourhood of $f_{\mathrm{rot,theory}}$. At comparatively high intensity ($\simeq 0.1\,\mu\mathrm{W\,mm^{-2}}$, green points), the linewidth is 12 kHz, whereas the calculated Doppler linewidth is 54 kHz. By reducing the source power successively, the line width decreases to 1.3 kHz (blue points). This clearly evidences power broadening. The latter linewidth is mostly due to residual power broadening. To obtain sufficient signal strength, we did not lift the Zeeman degeneracy completely and the spectrum contains the unresolved superposition of the pair T_+ and T_-.

Systematic shifts were computed or estimated, resulting in a frequency correction $\delta f_{\mathrm{rot,exp,syst}} = 0.0(3)$ kHz (see Methods). We obtain the rotational frequency

$$f_{\mathrm{rot,exp}} = 1,314,935.8280(4)_{\mathrm{stat}}(3)_{\mathrm{syst}}\ \mathrm{MHz} \quad (2)$$

The statistical uncertainty results from the experimental line centre resolution.

The value $f_{\mathrm{rot,exp}}$ is in agreement with the ab initio prediction $f_{\mathrm{rot,theory}}$. This represents the most accurate test of a molecular physics prediction, and is limited by the current uncertainty of the theory value, 8×10^{-10}.

The ab initio value $f_{\mathrm{rot,theory}}$ is based on the CODATA2014 values of the fundamental constants[26], in particular on the proton mass m_{p}. Among the stable fundamental particles of atomic physics, this is the particle that currently has the largest fractional mass uncertainty (9×10^{-11}). We can obtain a value for m_{p} from the present experiment by treating it as a fit parameter, while taking the other constants, m_{d}, m_{e}, R_{∞} and α, and their uncertainties from CODATA2014. The value then is

$$m_{\mathrm{p}} = 1.0072764669(13)\ \mathrm{u} \quad (3)$$

with fractional uncertainty 1.3×10^{-9}, where the statistical, the systematic and the theoretical error enter as a sum of squares. Our result is consistent with CODATA2014, and is obtained by a different measurement method. It is the most accurate result for m_{p} using molecular spectroscopy to date, and improves by a factor of 3.4 on the recent result[16].

Our experiment–theory agreement is a direct proof that the present method permits rotational frequency inaccuracy at the 9×10^{-10} level or better, without the necessity for corrections. The reasons for this are the long spectroscopy wavelength, the stretched-state transitions and the favourable conditions in the UHV ion trap, and not a particular insensitivity of the HD^+ test molecule to perturbations. Rotational transitions between stretched states, with Zeeman splittings comparable to the present one, are available in most species, owing to the structure of the underlying magnetic Hamiltonian and of the wavefunctions[25]. Therefore, similar inaccuracy levels should be achievable for numerous other molecular species.

The present work opens outstanding perspectives for precision physics. With improvements in signal strength, we expect that the spectroscopic resolution can be increased by at least one order, leading in addition to a systematic uncertainty $<3\times10^{-11}$ (see Methods). This will eventually allow testing of the ab initio prediction of the rotational frequency of the HD^+ molecular ion[27–30] with corresponding accuracy, then providing also a fairly direct test of the theory of the related molecular ions H_2^+ and D_2^+ and of antiprotonic helium. Eventually, the fundamental constants R_{∞}, m_{e}, m_{p} and m_{d} will become measurable at the 10^{-11} level by molecular spectroscopy. This complementary approach to the current ones will strengthen the overall consistency of this set of fundamental constants.

Our method opens up additional wide possibilities, for several reasons. Given the mass (m_{c}) of singly ionized laser-coolable atomic ions, molecular ions with a mass-to-charge-squared ratio $m/q^2 < m_{\mathrm{c}}/e^2$ can be confined inside the atomic ion cluster, in the rotational Lamb–Dicke regime. Employing, for example, the high-mass ytterbium ion $^{171}Yb^+$ as a coolant, many thousands of singly ionized ($q=e$) molecular species, not counting isotopologues, have a suitable mass. Many of these species exhibit a simpler spin structure than the test case used here, which can be advantageous in simplifying the spectrum and increasing state populations. A general method for preparing molecular ions in the ground rovibrational level ($v=0$, $N=0$) is cryogenic buffer gas cooling[31]. It is also applicable to homonuclear ions, including H_2^+ and D_2^+ (ref. [32]).

Finally, the present method should be applicable also to rotational stimulated Raman transitions driven by co-propagating waves and to two-photon vibrational transitions. The latter would be driven by counter-propagating waves f_1 and f_2 having a sufficiently small frequency difference $|f_1-f_2| < c\,/\,2\pi\delta x$, ensuring the LDR. It is particularly advantageous that, in diatomics, transitions exist for which f_1 and f_2 can be chosen to satisfy this condition and also to be near-resonant with a dipole-allowed transition to an intermediate rovibrational level, so that the two-photon transition rate is enhanced.

Methods

Methods, including statements of data availability and any associated accession codes and references, are available at https://doi.org/10.1038/s41567-018-0074-3.

Received: 4 October 2017; Accepted: 2 February 2018;
Published online: 26 March 2018

References

1. Raizen, M., Gilligan, J., Bergquist, J., Itano, W. & Wineland, D. Ionic crystals in a linear Paul trap. *Phys. Rev. A* **45**, 6493 –6501 (1992).
2. Waki, I., Kassner, S., Birkl, G. & Walther, H. Observation of ordered structures of laser-cooled ions in a quadrupole storage ring. *Phys. Rev. Lett.* **68**, 2007–2010 (1992).
3. Bowe, P. et al. Sympathetic crystallization of trapped ions. *Phys. Rev. Lett.* **82**, 2071–2074 (1999).
4. Barrett, M. D. et al. Sympathetic cooling of $^9Be^+$ and $^{24}Mg^+$ for quantum logic. *Phys. Rev. A* **68**, 042302 (2003).
5. Bressel, U. et al. Manipulation of individual hyperfine states in cold trapped molecular ions and application to HD^+ frequency metrology. *Phys. Rev. Lett.* **108**, 183003 (2012).
6. Berkeland, D. J., Miller, J. D., Bergquist, J. C., Itano, W. M. & Wineland, D. J. Laser-cooled mercury ion frequency standard. *Phys. Rev. Lett.* **80**, 2089–2092 (1998).
7. Townes, C. & Schawlow, A. *Microwave Spectroscopy* (Dover, New York, NY, 1975).
8. Jusko, P., Asvany, O., Wallerstein, A.-C., Brünken, S. & Schlemmer, S. Two-photon rotational action spectroscopy of cold OH^- at 1 ppb accuracy. *Phys. Rev. Lett.* **112**, 253005 (2014).
9. Schiller, S. & Korobov, V. Test of time-dependence of the electron and nuclear masses with ultracold molecules. *Phys. Rev. A.* **71**, 032505 (2005).
10. Shelkovnikov, A., Butcher, R. J., Chardonnet, C. & Amy-Klein, A. Stability of the Proton-to-Electron Mass Ratio. *Phys. Rev. Lett.* **100**, 150810 (2008).
11. Uzan, J.-P. Varying constants, gravitation and cosmology. *Living Rev. Relativ.* **14**, 2 (2011).
12. Godun, R. M. et al. Frequency ratio of two optical clock transitions in $^{171}Yb^+$ and constraints on the time variation of fundamental constants. *Phys. Rev. Lett.* **113**, 210801 (2014).
13. Huntemann, N. et al. Improved limit on a temporal variation of m_p/m_e from comparisons of Yb^+ and Cs atomic clocks. *Phys. Rev. Lett.* **113**, 210802 (2014).
14. Roth, B. et al. in *Precision Physics of Simple Atoms and Molecules. Lecture Notes in Physics* Vol. 745 (ed. Karshenboim S. G.) 205–232 (Springer, Berlin, Heidelberg, 2008).
15. Koelemeij, J. C. J., Roth, B., Wicht, A., Ernsting, I. & Schiller, S. Vibrational spectroscopy of HD^+ with 2-ppb accuracy. *Phys. Rev. Lett.* **98**, 173002 (2007).
16. Biesheuvel, J. et al. Probing QED and fundamental constants through laser spectroscopy of vibrational transitions in HD^+. *Nat. Comm.* **7**, 10385 (2016).
17. Winton, R. S. & Gordy, W. High-precision millimeter-wave spectroscopy with Lamb dip. *Phys. Lett. A.* **32**, 219–220 (1970).
18. Cazzoli, G. & Dore, L. Observation of crossing resonances in the hyperfine structure of the $J = 1 \leftarrow 0$ transition of $DC^{15}N$. *J. Mol. Spectrosc.* **143**, 231–236 (1990).
19. Winnewisser, G., Belov, S. P., Klaus, T. & Schieder, R. Sub-Doppler measurements on the rotational transitions of carbon monoxide. *J. Mol. Spectrosc.* **184**, 468–472 (1997).
20. Cazzoli, G. & Puzzarini, C. Sub-Doppler resolution in the THz frequency domain: 1 kHz accuracy at 1 THz by exploiting the Lamb-dip technique. *J. Phys. Chem. A* **117**, 13759–13766 (2013).
21. Dicke, R. H. The effect of collisions upon the Doppler width of spectral lines. *Phys. Rev.* **89**, 472–473 (1953).
22. Germann, M., Tong, X. & Willitsch, S. Observation of dipole-forbidden transitions in sympathetically cooled, state-selected, homonuclear diatomic molecular ions. *Nat. Phys.* **10**, 820–824 (2014).
23. Wolf, F. et al. Non-destructive state detection for quantum logic spectroscopy of molecular ions. *Nature* **530**, 457–460 (2016).

24. Chou, C. et al. Preparation and coherent manipulation of pure quantum states of a single molecular ion. *Nature* **545**, 203–207 (2017).
25. Bakalov, D., Korobov, V. & Schiller, S. Magnetic field effects in the transitions of the HD^+ molecular ion and precision spectroscopy. *J. Phys. B* **44**, 025003 (2011); corrigendum **45**, 049501 (2012).
26. Mohr, P. J., Newell, D. B. & Taylor, B. N. CODATA recommended values of the fundamental physical constants: 2014. *Rev. Mod. Phys.* **88**, 035009 (2016).
27. Korobov, V. I., Hilico, L. & Karr, J. P. Theoretical transition frequencies beyond 0.1 ppb accuracy in H_2^+, HD^+, and antiprotonic helium. *Phys. Rev. A* **89**, 032511 (2014).
28. Korobov, V. I., Hilico, L. & Karr, J.-P. $m\alpha^7$-order corrections in the hydrogen molecular ions and antiprotonic helium. *Phys. Rev. Lett.* **112**, 103003 (2014).
29. Korobov, V. I., Koelemeij, J. C. J., Hilico, L. & Karr, J.-P. Theoretical hyperfine structure of the molecular hydrogen ion at the 1 ppm level. *Phys. Rev. Lett.* **116**, 053003 (2016).
30. Korobov, V. I., Hilico, L. & Karr, J.-P. Fundamental transitions and ionization energies of the hydrogen molecular ions with few ppt uncertainty. *Phys. Rev. Lett.* **118**, 233001 (2017).
31. Hansen, A. K. et al. Efficient rotational cooling of Coulomb-crystallized molecular ions by a helium buffer gas. *Nature* **508**, 76–79 (2014).
32. Schiller, S., Kortunov, I., Hernández Vera, M., Gianturco, F. & da Silva, H. Quantum state preparation of homonuclear molecular ions enabled via a cold buffer gas: An ab initio study for the H_2^+ and the D_2^+ case. *Phys. Rev. A* **95**, 043411 (2017).
33. Bakalov, D., Korobov, V. I. & Schiller, S. High-precision calculation of the hyperfine structure of the HD^+ ion. *Phys. Rev. Lett.* **97**, 243001 (2006).
34. Shen, J., Borodin, A. & Schiller, S. A simple method for characterization of the magnetic field in an ion trap using Be^+ ions. *Eur. Phys. J. D.* **68**, 359 (2014).

Acknowledgements

This work has been partially funded by Deutsche Forschungsgemeinschaft project Schi 431/19-1. V.I.K. acknowledges support from the Russian Foundation for Basic Research under grant no. 15-02-01906-a. We thank U. Rosowski for important assistance with the frequency comb, A. Nevsky for assistance with a laser system, E. Wiens for characterizing H-maser instability, D. Iwaschko, R. Gusek and P. Dutkiewicz for electronics development, J. Scheuer and M. Melzer for assistance, and S. Schlemmer (Universität zu Köln) for equipment loans. We thank K. Brown (Georgia Institute of Technology) for useful discussions and suggestions.

Author contributions

S.A. and M.G.H. developed the apparatus and performed the experiments; S.A., M.G.H. and S.S. analysed the data; S.A., S.S. and V.I.K. performed theoretical calculations; S.S. conceived the study, supervised the work and wrote the paper.

Competing interests

The authors declare no competing interests.

Additional information

Supplementary information is available for this paper at https://doi.org/10.1038/s41567-018-0074-3.

Reprints and permissions information is available at www.nature.com/reprints.

Correspondence and requests for materials should be addressed to S.S.

Methods

Simulation of ion dynamics in Coulomb clusters. The spatial distribution of ions in a two-species Coulomb crystal is well known[35]. Given an elongated trap and electrode geometry, and for typical magnitudes of the radiofrequency voltages and of the end-cap voltages, a strongly prolate atomic ion cluster can result. Sympathetically cooled molecular ions, if lighter than the atomic coolant ions, and if fewer in number, are distributed in a string-like or tube-like volume, centred on the trap axis (z). (Equal charge states are assumed.) The boundary shapes of the two species' spatial distributions are constant in time.

Molecular dynamics simulations help to elucidate details, in particular effects of temperature and dynamics. We simulated two ion clusters. Cluster C1 contains $N_{Be^+}=2{,}000$ Be^+ ions that sympathetically cool $N=200$ HD^+ ions, resulting in a tubular configuration for the latter. C1 is similar to the experimentally produced clusters (Fig. 1). A smaller cluster (C2) was modelled for comparison: with $N=50$, $N_{Be^+}=500$, the molecular ions arrange as a string. The simulations are performed in the pseudopotential approximation, since the micromotion of HD^+ ions gives only small corrections (here, the q-parameter is 0.15). The simulations extended over 5 ms. The equilibrium secular temperature T of the molecular ions is determined by the assumed cooling and heating rate parameters, which are varied in order to exhibit the temperature dependence of the clusters' properties[36]. A key feature of large clusters such as C1 is that even at the lowest temperatures achievable experimentally by sympathetic cooling, $T\simeq 10$–30 mK, the ions' positions are not completely 'frozen'. Instead, the ions diffuse through the cluster volume, with the diffusion speed being a function of temperature[36].

The ion motion characteristics can be analysed in detail. One characteristic is the coordinate r.m.s. variation, defined as $\Delta\xi=\langle\Delta\xi_i\rangle$, $\Delta\xi_i^2=\overline{\xi_i(t)^2}-\overline{\xi_i(t)}^2$, where i is the ion number, $\xi=x,y,z$, the over-bar denotes the time average and $\langle\ldots\rangle=N^{-1}\sum_{i=1}^{N}\ldots$ denotes the ensemble average. The values for C1 put in evidence transverse confinement and diffusion features: whereas for motion along the trap axis $\Delta z_{C1}=(41, 142, 206)$ μm over a time interval of 5 ms, at $T=(12, 33, 67)$ mK, respectively, the transverse excursions are $\Delta x_{C1}=\Delta y_{C1}=(8.4, 8.6, 9.0)$ μm. These latter values are significantly smaller than $\lambda_{rot,min}/2\pi$. In Fig. 2a,b, we show some details of HD^+ ion motion, the time-averaged spatial distribution of a tube-like cluster and the spectral density of the x coordinate. Two characteristics of the spectral density related to the increasing localization with decreasing temperature are: the increasing strength for near-zero frequency; and the strong drop in spectral density at frequencies larger than 0.81 MHz, the secular frequency. At the smallest simulated temperatures, the drop is stronger for the string-like ion cluster than for the tube-like cluster. For the former, the secular frequency eventually becomes the largest frequency of motion possible, because it is the frequency of the small (thermally driven) oscillations around the equilibrium positions. For the latter, the ions can still perform azimuthal motion and thus the spectrum differs qualitatively.

If the ions' coordinates $x_i(t)$ were Gaussian random variables, $L(0)$ would simplify to $L_g(0)=\langle\exp(-(2\pi\Delta x_i/\lambda)^2)\rangle$ (ref. [37]). Since in clusters of the sizes as in C1, C2, most ions behave similarly, $L_g(0)\simeq\exp(-(2\pi\Delta x/\lambda)^2)$. This expression explicitly shows the wavelength dependence, and is presented as dashed lines in the figure. The Gaussian assumption is well satisfied when the number of molecules N is reduced so far (cluster C2) that they arrange approximately like a string along the z axis, since their x histogram is then found to be Gaussian. For C2, $\Delta x_{C2}=\Delta y_{C2}\simeq(1.7, 3.0, 4.1)$ μm at $T=(12, 33, 67)$ mK increase approximately with the square root of the temperature, and thus more strongly in relative terms than for C1. This leads to a more pronounced variation of $L(0)$ with temperature than for C1 (see Fig. 2d). The small values Δx_{C2}, Δy_{C2} lead to a substantial $L(0)\simeq 0.3$ already for $\lambda\simeq 10$ μm when $T=13$ mK.

For the C1 cluster, the Gaussian assumption is not correct (see the histogram in Fig. 2a); therefore, deviations between $L_g(0)$ and $L(0)$ are visible in Fig. 2d for intermediate and small wavelengths. Heuristically, we find that the expression $L_{sp}(0)=J_0(2\pi\sqrt{2}\,\Delta x/\lambda)^2$, the result for a single ion harmonically oscillating along the x axis[38], provides a better description of the exact values because of the similarity in the probability distributions of the x coordinate values.

Thus, the simulations indicate that even for only moderately cold ensembles ($T\simeq 70$ mK) and for a relatively small rotational wavelength $\lambda_{rot,min}=228$ μm ($f_{rot,max}=1.3$ THz), strong signatures of Lamb–Dicke confinement in rotational spectroscopy with transverse incidence can be expected. For string-like ion clusters, a similar signature might be possible also for axial irradiation, but only at the lowest temperatures ($T\simeq 10$ mK), when ion position changes are infrequent.

Experimental apparatus. The ion trap apparatus used in the present work, shown in Supplementary Fig. 1, is based on the device used previously[5,39–41], and upgraded in several respects: fully computer-controlled operation, accurate magnetic field control via solenoid pairs, improved frequency stabilization of the rotational cooling lasers L-RC1 and L-RC2, and improved terahertz source frequency control.

The vacuum chamber housing the ion trap provides UHV conditions (3×10^{-11} mbar), minimizing spectral broadening and shifts due to ion–background gas collisions. Electron impact ionization inside the ion trap volume is used to generate beryllium ions from Be atoms emitted by a hot filament and HD^+ ions from HD gas injected into the chamber. A 313 nm radiation laser cools the beryllium ions that sympathetically cool the HD^+ ions, resulting in a structured ion cluster as shown in Fig. 1. Subsequently, radiation fields at 5.48 μm and 2.71 μm perform rotational cooling. The 1.3 THz radiation for rotational spectroscopy propagates at 90 degrees with respect to the ion trap axis and thus the ion cluster axis, in order to provide the LDR. The beam radius at the centre of the trap is approximately 1 mm. A CCD (charge-coupled device) camera images the cluster's spatial structure, allowing for a direct observation of the spatial confinement and also comparison with molecular dynamics simulations. The photo-multiplier tube detects the fluorescence of the Be^+ ions, and also provides the signal for the spectroscopy.

The terahertz system consists of a hydrogen maser, whose frequency, $f_H\simeq 1.4$ GHz, is down-converted to 10 MHz and then used as a reference for a microwave synthesizer operating at $f_{mmw}/72=18.262$ GHz. Its output is converted in a ×72 multiplier/amplifier chain to $f_{mmw}=f_{rot}=1.31$ THz (ref. [42]). We verified the high spectral purity of the terahertz wave at the intermediate frequency 18.251 GHz, close to $f_{mmw}/72$. The set-up used is shown in Supplementary Fig. 2 (inset). The repetition rate $f_{rep}\simeq 250$ MHz of a fibre-based optical frequency comb is stabilized by phase-locking the beat frequency between an ultrastable reference laser at 1.5 μm (L-ULE, with optical frequency f_{ULE}[43]) and a nearby comb mode (mode number $n\simeq 7.8\times10^5$) to a (maser-referenced) direct digital synthesizer (DDS) set at $f_{DDS}=50$ MHz, by controlling the repetition rate. The comb's carrier-envelope offset frequency f_{CEO} is independently stabilized to the H-maser. The absolute frequency stability of the reference laser is therefore transferred to the repetition rate, $f_{rep}=(f_{ULE}-f_{DDS}-f_{CEO})/n$. Comb radiation at 1.5 μm is detected by a fast photo-detector, and a radiofrequency signal arising from the 73rd harmonic of the repetition rate, $f_{rep}\times 73$, is generated. This harmonic is chosen because it can be set close to $f_{mmw}/72$. The difference frequency between $f_{rep}\times 73$ and $f_{mmw}/72$ is generated using a mixer and is analysed with a fast Fourier transform-based spectrum analyser. Supplementary Fig. 2 shows the linewidth of the difference frequency signal, which is 86 mHz. On the basis of this value and previous characterizations[42], we estimate a linewidth <10 Hz at 1.3 THz. We can also infer the long-term frequency stability of the terahertz wave, by comparing the maser frequency to a Global Positioning System (GPS)-derived 1 pulse per second signal and to a cryogenic silicon optical resonator[44]. The residual instability is negligible ($<1\times10^{-13}$ for integration times $\tau>10$ s) and so is drift.

Laser rotational cooling. In the present experiment, when molecular ions are generated and trapped and reach thermal equilibrium, the ($v''=0$, $N''=0$) level's population is ≃10%, and thus only ≃1% is in a single state $|g,m_F^{\,*}\rangle$. Therefore, before spectroscopy, we apply rotational laser cooling[40] (lasers L-RC1, L-RC2 in Supplementary Fig. 1), to significantly increase the population in ($v''=0$, $N''=0$), a procedure that also increases the population in the Zeeman states $|g,m_F^{\,*}\rangle$ to a level that can be observed.

We apply two laser fields that drive the fundamental vibrational transition ($v''=0$, $N''=2$) → ($v'=1$, $N'=1$), and the overtone vibrational transition ($v''=0$, $N''=1$) → ($v'=2$, $N'=0$), respectively. Owing to quantum mechanical selection rules, repeated absorption–spontaneous emission cycles transfer the majority of the ion population into the ground state ($v=0$, $N=0$).

The fundamental transition at 5.48 μm is driven by a quantum cascade laser (L-RC2 in Supplementary Fig. 1), whose frequency is stabilized to the side of a fringe of an NH_3 molecular transition. The overtone vibrational transition is excited by a distributed feedback laser at 2.71 μm (L-RC1 in Supplementary Fig. 1). The laser is frequency-stabilized to a CO_2 gas transition using an offset locking technique[45] to bridge the frequency gap between the CO_2 and the HD^+ transition frequencies.

Experimental sequence. The preparation and spectroscopy sequence consists of the following steps: (1) HD^+ generation by electron impact ionization; (2) impurity ion removal procedures; (3) rotational cooling for $t_{rc}=35$ s; (4) secular excitation for $t_{se}=3$ s, with rotational cooling lasers on; (5) during $t_{det}=3$ s, the rotational cooling lasers are blocked, while terahertz radiation and the 1.42 μm and 266 nm waves for resonance-enhanced multi-photon dissociation are on; (6) secular excitation during t_{se}. The signal is obtained from the difference in Be^+ fluorescence recorded during intervals (4) and (6).

The magnetic field is set to 0.11 mT along the trap axis z, except during step (5), where it is set to a smaller value B, sufficient to produce Zeeman splitting of most components of the studied transition. The sequence is repeated a number of times sufficient to obtain a reasonable signal-to-noise ratio. Be^+ ions are reloaded every 100 to 150 sequences.

Rotational transition. The fundamental rotational transition of the molecular ion used here has an important spin structure because of the electron and nuclear magnetic moments[33]. Whereas in the ground rovibrational level ($v''=0$, $N''=0$) they give rise to four spin states (having total angular momentum $F''=0$, 1, 2), in the first excited rotational level ($v'=0$, $N'=1$) the number increases to ten spin states (having $F'=0$, 1, 2, 3), because of the additional presence of rotational angular momentum $N''\neq 0$. Figure 3 shows the two spin states relevant to the spectroscopy of this work (for a complete diagram, see Fig. 2 in ref. [41]). A controllable magnetic field lifts the total angular momentum projection (m_F) degeneracies. We address transitions between two individual Zeeman components

$|g, m_{F''}\rangle$ of the $F''=2$ spin state of the $N''=0$ level, and two components $|e, m_F\rangle$ of the $F'=3$ spin state of the $N'=1$ level. These are the transitions T_+: $m_{F''}=2 \rightarrow m_{F'}=3$ and T_-: $m_{F''}=-2 \rightarrow m_{F'}=-3$, shown by green arrows in Fig. 3.

Ab initio theory of the HD$^+$ rotational transition. The transition frequency $f_{\mathrm{rot,theory}}$ involves two contributions. The first is the spin-averaged frequency $f_{\mathrm{spin\text{-}avg}}$. We have computed it with high accuracy using the same technique as in ref. [30], obtaining

$$f_{\mathrm{spin-avg}} = 1,314,925.752627(18)\ \mathrm{MHz}$$

CODATA2014 values[26] have been used and the relative uncertainty indicated is that due to theory, 1.4×10^{-11}. The second contribution is the hyperfine shift f_{spin} due to spin interactions (including coupling with the total orbital angular momentum), $f_{\mathrm{spin}} = [E_{\mathrm{spin}}(|e\rangle) - E_{\mathrm{spin}}(|g\rangle)]\ /\ h$. Here, $E_{\mathrm{spin}}(|e\rangle)$ and $E_{\mathrm{spin}}(|g\rangle)$ are the hyperfine spin energy shifts for the lower and upper states, respectively. So far, they have been calculated only within the Breit–Pauli approximation[33]. For the stretched states $|g, m_{F''}=\pm2\rangle$ and $|e, m_{F'}=\pm3\rangle$, including the Zeeman energy in a finite magnetic field B, we have previously derived the algebraic expression (equation (6) in ref. [25]),

$$\begin{aligned} E_{\mathrm{spin}}(v,N,F=N+2,m_F=\pm F,B)/\ h = {} & E_4\ /\ 4 + E_5\ /\ 2 \\ & + (E_1+E_2+2E_3+E_6+2E_7+2E_8+E_9)N\ /\ 2 \\ & - (2E_6+4E_7+4E_8+2E_9)N^2\ /\ 2 \\ & \pm (2E_{10}N+E_{11}+2E_{12}+E_{13})B\ /\ 2 \end{aligned}$$

where $E_i = E_i(v,N)$ are the coefficients of the effective spin Hamiltonian[25,33] and $E_{10}=E_{10}(v,N\geq1)\simeq-5\,\mathrm{kHz\,mT^{-1}}$ is the weakly v, N-dependent strength of the rotational Zeeman interaction $\mathbf{N}\cdot\mathbf{B}$. E_{11}, E_{12} and E_{13} are particle magnetic constants, with $a=(E_{11}+2E_{12}+E_{13})/2\simeq14.0\,\mathrm{MHz\,mT^{-1}}$. Since the $F''=2\rightarrow F'=3$ transition keeps the spin function untouched, the hyperfine shift f_{spin} is most sensitive to the electron spin–orbit interaction $E_1(v=0,N=1)(\mathbf{s}_e\cdot\mathbf{N})$, where $E_1(v=0,N=1)\simeq32\,\mathrm{MHz}$ (ref. [33]). The spin–spin interactions, proportional to E_4 and E_5, which are known with much higher accuracy than the other coefficients[29], give a much smaller contribution to f_{spin}, due to the similarity of the spin wavefunctions in $|g\rangle$, $|e\rangle$ that leads to a substantial cancellation. The hyperfine shift of the transitions $T_\pm$ is

$$f_{\mathrm{spin}} = 10.0747(10)\ \mathrm{MHz} \pm E_{10}(v=0,N=1)B \qquad (4)$$

Summing both above contributions, we obtain equation (1).

It is important to note that the theoretical considerations of the spin-averaged and the hyperfine spin shift contributions to $f_{\mathrm{rot,theory}}$ have recently been confirmed through a comparison, respectively, with one particular rovibrational transition frequency of HD$^+$ at the 1.1×10^{-9} level[16] and with several spin transition frequencies (that is, radiofrequency transitions) of H_2^+ at the 10^{-6} level[29].

The particular sensitivity of the observed transition to the accuracy of the effective spin Hamiltonian is characteristic for rotational transitions. For vibrational transitions, the much larger ratio of $f_{\mathrm{spin\text{-}avg}}$ to f_{spin} reduces the sensitivity to the latter significantly. This is the case for the most intensive hyperfine components of the transitions (for which $|f_{\mathrm{spin}}|<100$ MHz), and the Breit–Pauli approximation is then in most cases sufficient to guarantee a fractional uncertainty of the total transition frequency comparable to the fractional uncertainty of the theoretical spin-averaged frequency.

To improve the 1 kHz theoretical uncertainty of f_{spin}, it will be necessary to calculate the higher-order corrections to the coefficients E_1 to E_7. It is expected that a calculation of their contributions of relative order α^4 partially of α^5 will be possible, with reduction of the uncertainty in f_{spin} by a factor of up to 10^3 and thus in $f_{\mathrm{rot,theory}}$ to the 1×10^{-11} level.

Systematic shifts. We have previously computed most relevant sensitivities of the rotational transition to external perturbations: Zeeman shift[25], electric quadrupole shift[46], d.c. Stark shift, black-body radiation shift, and spin-state dependences of the d.c. Stark and light shift[47]. For the experimental parameters of our trap, the cluster shape, and the moderate intensities of the radiation fields, the shifts of the transitions $T_\pm$ are all small, except for the linear Zeeman shift (the quadratic Zeeman shift is zero). In detail we have the following contributions.

(1) Since the orientation of the quantization axis and the populations of the lower Zeeman states are unknown, we assign a Zeeman uncertainty equal to half the Zeeman splitting of T_+ and T_-, 0.22 kHz. (2) The d.c. Stark shift has been computed taking into account ion trajectories and Coulomb fields, also allowing for d.c. offset potentials, and is less than 10 Hz. (3) Collision shifts related to background gas are negligible due to the UHV conditions, and effects of non-thermal velocity distribution[16] are considered negligible because of the spectroscopy technique used here and the magnitude of the hyperfine splittings. (4) The light shift induced by the 266 nm dissociation laser (35 mW power) has been evaluated by performing an accurate calculation of the a.c. polarizabilities of the lower and upper rotational levels using the procedure described in ref. [47]. We obtained the scalar (s) and tensor (t) polarizabilities $\alpha_s(v=0,N=0(1),\lambda=266.0\,\mathrm{nm})=3.677(3.687)$, $\alpha_t(v=0,N=0(1),\lambda=266.0\,\mathrm{nm})=0(-1.044)$, in atomic units. For the considered transitions, the shift is 7 (40) Hz. (5) Black-body radiation shift and electric quadrupole shift are negligible.

In total, we obtain a frequency correction of $\delta f_{\mathrm{rot,exp,syst}}=0.0(3)\,\mathrm{kHz}$.

In future studies, any light shifts from the dissociation laser and from the 1.4 μm laser could be avoided by applying these lasers only after the rotational excitation. If the Zeeman pair were split and resolved, the Zeeman shift uncertainty should be reduced at least tenfold. This would then allow a total systematic uncertainty of $<3\times10^{-11}$.

Outlook. We note that radiation sources of appropriate spectral purity and stability can be implemented not only using an H-maser as a reference but also more simply and accessibly using a GPS-steered high-performance quartz oscillator. For most molecules, the fundamental rotational transition frequency is smaller than 1 THz, which simplifies the source further. In a complementary direction, the method could also be applied to other rotational transitions $N''>0\rightarrow N'=N''+1$, with correspondingly higher frequencies and thus potentially higher fractional spectral resolution. It is possible that two-photon[48] and electric quadrupole rotational transitions could also become accessible.

Data availability. The data that support the plots within this paper and other findings of this study are available from the corresponding author upon reasonable request.

References

35. Hornekær, L., Kjærgaard, N., Thommesen, A. M. & Drewsen, M. Structural properties of two-component Coulomb crystals in linear Paul traps. *Phys. Rev. Lett.* **86**, 1994 (2001).
36. Zhang, C. B., Offenberg, D., Roth, B., Wilson, M. A. & Schiller, S. Molecular-dynamics simulations of cold single-species and multispecies ion ensembles in a linear Paul trap. *Phys. Rev. A* **76**, 012719 (2007).
37. Cramér, H. *Random Variables and Probability Distributions* (Cambridge Univ. Press, Cambridge, 1970).
38. Berkeland, D. J., Miller, J. D., Bergquist, J. C., Itano, W. M. & Wineland, D. J. Minimization of ion micromotion in Paul trap. *J. Appl. Phys.* **83**, 5025–5033 (1998).
39. Blythe, P., Roth, B., Fröhlich, U., Wenz, H. & Schiller, S. Production of ultracold trapped molecular hydrogen ions. *Phys. Rev. Lett.* **95**, 183002 (2005).
40. Schneider, T., Roth, B., Duncker, H., Ernsting, I. & Schiller, S. All-optical preparation of molecular ions in the rovibrational ground state. *Nat. Phys.* **6**, 275–278 (2010).
41. Shen, J., Borodin, A., Hansen, M. & Schiller, S. Observation of a rotational transition of trapped and sympathetically cooled molecular ions. *Phys. Rev. A* **85**, 032519 (2012).
42. Schiller, S., Roth, B., Lewen, F., Ricken, O. & Wiedner, M. Ultra-narrow-linewidth continuous-wave THz sources based on multiplier chains. *Appl. Phys. B* **95**, 55–61 (2009).
43. Wiens, E., Nevsky, A. Y. & Schiller, S. Resonator with ultrahigh length stability as a probe for equivalence-principle-violating physics. *Phys. Rev. Lett.* **117**, 271102 (2016).
44. Wiens, E. et al. A silicon single-crystal cryogenic optical resonator. *Opt. Lett.* **39**, 3242–3245 (2014).
45. Nevsky, A. Y. et al. Robust frequency stabilization of multiple spectroscopy lasers with large and tunable offset frequencies. *Opt. Lett.* **38**, 4903–4906 (2013).
46. Bakalov, D. & Schiller, S. The electric quadrupole moment of molecular hydrogen ions and their potential for a molecular ion clock. *Appl. Phys. B* **114**, 213–230 (2014).
47. Schiller, S., Bakalov, D., Bekbaev, A. K. & Korobov, V. I. Static and dynamic polarizability and the Stark and blackbody-radiation frequency shifts of the molecular hydrogen ions. *Phys. Rev. A* **89**, 052521 (2014).
48. Constantin, F. L. THz/infrared double resonance two-photon spectroscopy of HD$^+$ for determination of fundamental constants. *Atoms* **5**, 38 (2017).